Available online at www.sciencedirect.com

ScienceDirect

Geochimica et Cosmochimica Acta 316 (2022) 41–58

Geochimica et Cosmochimica Acta

www.elsevier.com/locate/gca

Clumped isotopes in modern marine bivalves

Damien Huyghe [a,b,c,*], Mathieu Daëron [d], Marc de Rafelis [b], Dominique Blamart [d], Mathieu Sébilo [e,f], Yves-Marie Paulet [g], Franck Lartaud [a]

[a] *Sorbonne Université, Laboratoire d'Ecogéochimie des environnements benthiques (LECOB), Observatoire Océanologique, F-66650 Banyuls-sur-mer, France*

[b] *Géosciences Environnement Toulouse (GET), Université Paul Sabatier Toulouse 3, 14 Avenue Edouard Belin, 31400 Toulouse, France*

[c] *Mines ParisTech, PSL University, Centre de Géosciences, 35 rue St Honoré, 77305 Fontainebleau Cedex, France*

[d] *Laboratoire des Sciences du Climat et de l'Environnement, LSCE/IPSL, CEA-CNRS-UVSQ, Université Paris-Saclay, Bât 714, CEA-Orme des merisiers RD 128, 91191 Gif-Sur-Yvette Cedex, France*

[e] *Sorbonne Université, Institut d'Ecologie et des Sciences de l'Environnement de Paris (IEES Paris), CNRS, F-75005 Paris, France*

[f] *Université de Pau et des Pays de l'Adour, E2S UPPA, IPREM (Institut des Sciences Analytiques et de Physico-Chimie pour l'Environnement et les Matériaux), Pau, France*

[g] *IUEM-UBO, UMR CNRS 6539, Lab. Sciences de l'Environnement Marin (LEMAR), Technopôle Brest-Iroise, Place N. Copernic, 29280 Plouzané, France*

Received 25 January 2021; accepted in revised form 16 September 2021; Available online 24 September 2021

Abstract

Oxygen-isotope measurements of fossil carbonates remain the most common method for paleoclimatic temperature reconstructions. A well-known limitation of this approach is the influence of the oxygen isotope composition of water in which mineralization occurs, which may vary significantly through space and time, and is often difficult to constrain precisely. Carbonate clumped-isotope thermometry is an alternative approach applicable to many carbonates. It is based on measurements of Δ_{47} (a tracer of small statistical anomalies in the abundance of rare, doubly-substituted carbonate isotopologues), and requires no independent information on the oxygen-isotope composition of parent waters. Here, we report new calibration observations of clumped isotopes in four species of calcitic marine bivalves (*A. colbecki*, *N. cochlear*, *S. cucullata*, *M. gigas*) from various ecosystems including coastal and deep-sea environments, with calcification temperatures ranging from −2 °C to 27 °C and very different amplitudes of seasonal temperature variability. At two localities with large seasonal temperature variability, calcification time intervals were constrained using a sclerochronological approach to test whether seasonal gradients of temperature can be accurately quantified based on Δ_{47} measurements.

Our results indicate that the mature bivalves we analyzed have clumped-isotope compositions entirely consistent with earlier calibration studies processed in the I-CDES reference frame and based on biogenic/abiotic/synthetic materials. By contrast, juvenile *M. gigas* oysters yield substantially lower Δ_{47} values than expected based on their calcification environments, suggesting that their early growth phase is associated with yet poorly understood isotopic biases affecting both $\delta^{18}O$ and Δ_{47} values. The link between seawater temperatures and bivalve Δ_{47} values is thus potentially applicable to seasonal reconstructions, but only if shell sections formed in cold seasons are precisely identified and precisely sampled, and taking into account that winter calcification is likely to be biased due to reduced growth rate. Moreover, the excellent agreement between our observations and the existing I-CDES calibrations further demonstrates the efficacy of the I-CDES standardization approach,

---

* Corresponding author at: Mines ParisTech, PSL University, Centre de Géosciences, 35 rue St Honoré, 77305 Fontainebleau Cedex, France.

E-mail address: damien.huyghe@mines-paristech.fr (D. Huyghe).

https://doi.org/10.1016/j.gca.2021.09.019

0016-7037/© 2021 Elsevier Ltd. All rights reserved.

and adds to the evidence that many different types of carbonates conform to statistically indistinguishable relationships between Δ_{47} and crystallization temperature.

© 2021 Elsevier Ltd. All rights reserved.

Keywords: Clumped isotopes; Mollusk; Paleoclimate; Temperature

1. INTRODUCTION

The oxygen-isotope composition of carbonate minerals has long remained the most common tool for environmental paleotemperature reconstructions. Its general principle rests on the fact that the oxygen-18 composition ($\delta^{18}O$) of carbonates varies with mineralization temperature. A noteworthy limitation of this method is that carbonate $\delta^{18}O$ values also depend on the isotopic composition of ambient water ($\delta^{18}O_w$), which often varies both in space, as it is function of the latitude and the balance between evaporation and precipitation (i.e., salinity) and in time, e.g., as a function of the glacial effect (i.e., the global fraction of water stored as continental ice). Thus, local $\delta^{18}O_w$ values are often difficult to quantify precisely, which constitutes a large source of uncertainty in past seawater temperature reconstructions (Shackleton, 1967; Cramer et al., 2011). Additional issues to consider are to what extent oxygen isotopes, particularly in biogenic carbonate, may record other parameters beyond temperature and water $\delta^{18}O$, and whether/how calibration relationships between calcification temperature and oxygen isotopes vary between different taxa.

Alternative paleotemperature proxies were developed over the last few decades, such as trace element ratios (e.g., Mg/Ca, Sr/Ca, Li/Mg) in biocarbonates, or organic tracers such as alkenones and TEX_{86} (Prahl and Wakeham, 1987; Schouten et al., 2007; Gentry et al., 2008; Mouchi et al., 2013; Rollion-Bard and Blamart, 2015). These approaches yield promising results, but they are not without limitations, particularly concerning their precision, accuracy, and applicability to various settings. For examples, Mg/Ca, one of the most used temperature proxies in bivalve shells, exhibits various temperature relationships for different oyster species and/or between younger and older specimens, and is heavily reliant on seawater composition changes, making difficult its use for past climate reconstructions (see review in Mouchi et al., 2013; Tynan et al., 2017).

Clumped-isotope carbonate thermometry is an alternative isotopic method constraining the crystallization temperature of carbonate minerals. It is based on the measurement of subtle statistical anomalies (Δ_{47}) in the abundance of doubly substituted carbonate isotopologues such as $^{13}C^{18}O^{16}O^{16}O$, relative to a purely stochastic distribution of isotopes (Ghosh et al., 2006; Eiler, 2011). For fundamental thermodynamic reasons, Δ_{47} values are expected to decrease systematically with crystallization temperature (Schauble et al., 2006). A notable advantage of this approach compared to others (e.g., $\delta^{18}O$ or Mg/Ca) is the fact that clumped-isotope reconstructions do not require any knowledge on seawater composition ($\delta^{18}O_w$). Combining Δ_{47} and $\delta^{18}O$ measurements of marine carbonates thus makes it possible to constrain past values of both seawater temperature and $\delta^{18}Ow$.

Over the past 15 years, many studies have documented the relationship between Δ_{47} values and mineralization temperatures for a broad variety of materials, including inorganic carbonates (e.g., Ghosh et al., 2006; Daëron et al., 2011; Kele et al., 2015; Bonifacie et al., 2017; Kelson et al., 2017) and biogenic carbonates such as foraminifera (Tripati et al., 2010; Grauel et al., 2013; Peral et al., 2018; Piasecki et al., 2019; Meinicke et al., 2020), coccoliths (Tripati et al., 2010; Katz et al., 2017), marine mollusks (Eagle et al., 2013; Henkes et al., 2013; Petrizzo et al., 2014) and land snails (Zaarur et al., 2011; Zhai et al., 2019). Overall, these studies suggest that, except for some specific types of carbonates such as corals (Thiagarajan et al., 2011; Spooner et al., 2016), brachiopods (Henkes et al., 2013; Came et al., 2014; Bajnai et al., 2018), or speleothems (e.g., Affek et al., 2008; Daëron et al., 2011; Affek and Zaarur, 2014; Meckler et al., 2015), Δ_{47} values in many types of natural carbonates are quasi-exclusively controlled by calcification temperature, to the exclusion of other environmental parameters such as water $\delta^{18}O$, salinity or pH.

Clumped-isotope carbonate thermometry is still relatively young, however. Precisely comparing Δ_{47} values measured in different laboratories has historically been somewhat problematic, but this issue has rapidly and consistently improved over the past decade (Dennis et al., 2011, Defliese et al., 2015; Daëron et al., 2016; Schauer et al., 2016; Fernandez et al., 2017; Bonifacie et al., 2017; Bernasconi et al., 2018; Petersen et al., 2019), culminating in the results of the InterCarb inter-comparison exercise (Bernasconi et al., 2021), which demonstrated that Δ_{47} measurements performed in 22 different laboratories using very different methods, then normalized to the "InterCarb Carbon Dioxide Equilibrium Scale" (I-CDES) using a common set of carbonate reference materials, are fully consistent within analytical errors.

Compared to other taxonomic groups such as foraminifera, relatively few studies of clumped isotopes in bivalves have been published so far. Bivalves are however widely used to constrain paleo-temperature in the littoral realm, as most species calcify shell material quasi-continuously throughout the year, allowing for the reconstruction of past seasonal variability (Purton and Brasier, 1997; Kirby et al., 1998; Kobashi et al., 2001; Harzhauser et al., 2010; Briard et al., 2020; Uvanović et al., 2021). Several clumped isotopes calibrations have already been established for marine mollusks (Eagle et al., 2013; Henkes et al., 2013; Petrizzo et al., Caldarescu, 2014). However, directly using these past results and quantita-

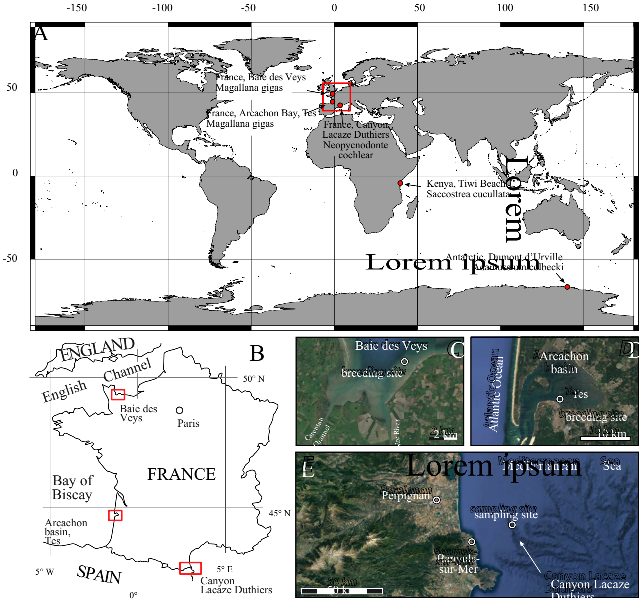

Fig. 1. A: Location of the sampling sites of the mollusks analyzed in this work. B: Location of the French sites where bivalves were sampled, corresponding to C: the Baie des Veys in Normandy, D: Tes in the Arcachon basin, and E: the Lacaze-Duthiers Canyon in the northwestern Mediterranean Sea.

tively comparing them to modern analyses remains challenging due to the standardization issues mentioned above. Moreover, despite promising potential for paleoclimate reconstructions, the use of clumped isotopes for reconstructing past seasonal contrasts has received little attention so far, even if some works showed the high potential for seasonal reconstruction with Δ_{47} at high-resolution (Hren et al., 2013; Ghosh et al., 2018; Van Plantinga and Grossman, 2018; Zhang et al., 2018; Briard et al., 2020; Caldarescu et al., 2021; de Winter et al., 2021). Among technical limitations, Δ_{47} generally requires an amount of carbonate powder unsuitable for seasonal analyses (de Winter et al., 2018). But to date, we still lack this type of approach on specimens from the field. Moreover, even if we do have examples of clumped measurements for some species, there are a lot of type of bivalves, living in various environments and characterized by different calcification behaviors. Therefore, calibrations on other species are required.

The present study aims to reassess the Δ_{47} calibration for marine mollusk shells, robustly anchored to the I-CDES. We selected specimens characterized by well-constrained growth conditions, allowing a precise report of clumped-isotope compositions with growth, using Δ_{47} values normalized by comparison to three international carbonate reference materials ETH-1, ETH-2 and ETH-3 (Bernasconi et al., 2021). By combining clumped-isotope measurements with a sclerochronological study of the analyzed shells, we assess whether seasonal gradients of temperature may be reliably derived from Δ_{47} in marine mollusk shells, thus potentially constraining paleo-environments at the intra-annual scale.

2. SPECIES AND SAMPLING SITES

Calibrating the clumped-isotope thermometer in mollusk shells requires reliable constraints on calcification temperatures. Specimens analyzed here were sampled from localities where seawater temperatures were monitored continuously except for one site. Thirty-one individual specimens of four bivalve species were analyzed for carbon-13, oxygen-18 and clumped isotopes, with water depths ranging from 0 to 270 m, and calcification temperatures from −1.8 °C to 27 °C (Table 1). All shells were sampled alive from their natural environments, avoiding aquaria culture experiments which may induce strong deviation in shell oxygen isotopes compared from predicted equilibrium, likely due to changes in growth rates that result in kinetic effects (Owen et al., 2002). A subset of these samples (Ad, PY, TW) was previously described by Daëron et al. (2019), in the context of a comparison between biogenic carbonates and slow-growing inorganic calcites from Devils Hole and Laghetto Basso. Table 1 lists all bivalve samples analyzed in the present study, grouped by species, locality, shell growth period, and calcification temperature.

2.1. Adamussium colbecki

Three specimens of the Antarctic scallop species *Adamussium colbecki* were collected by scuba divers in January 2007 at the French Antarctic station Dumont d'Urville (Fig. 1; 66°39.46S, 140°0.5E). The shells were collected from a depth of 15 m. Sensors deployed at this depth measured a mean annual seawater temperature of

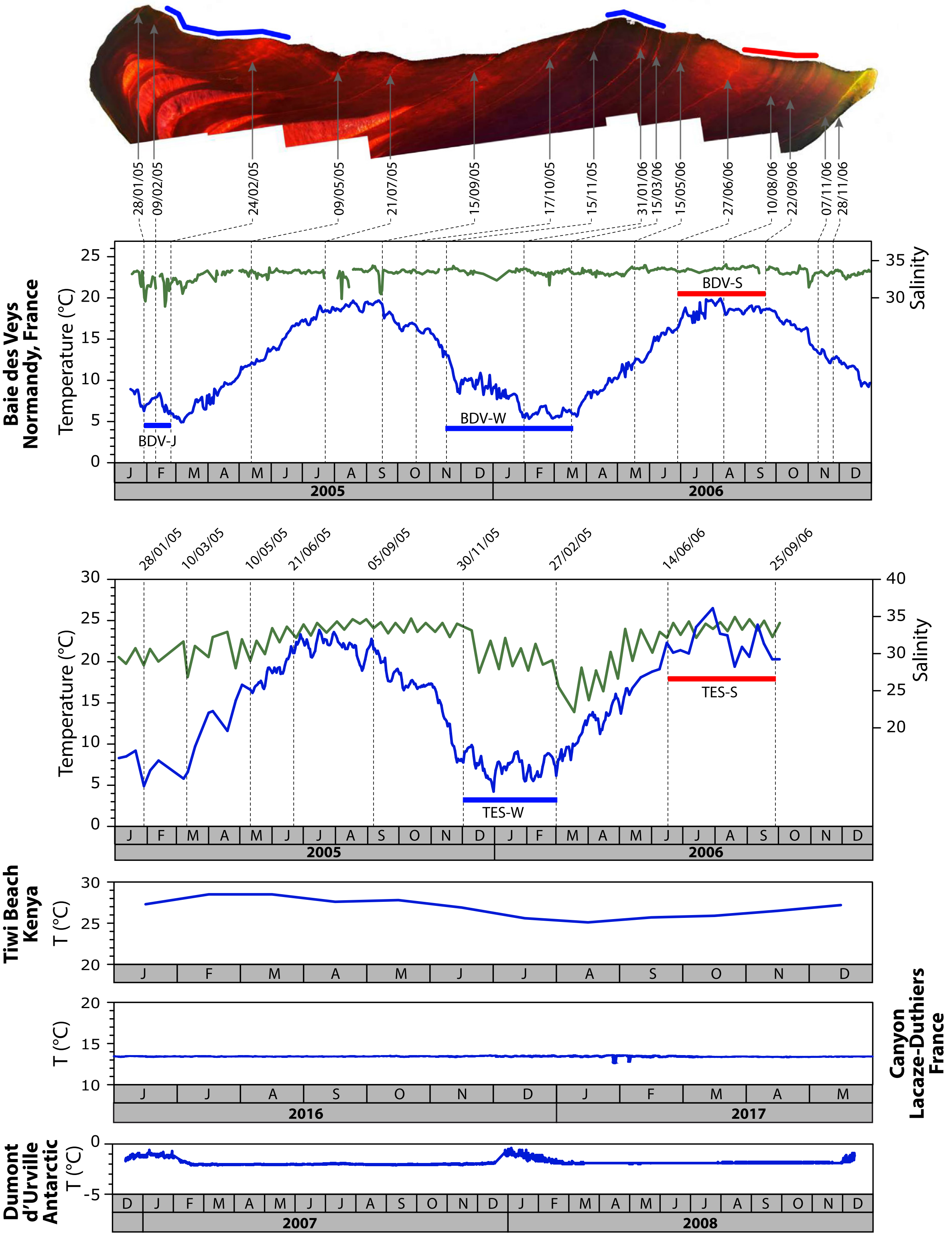

Fig. 2. Temperature and salinity of the sampling sites of the mollusks. Temperature at the Dumont d'Urville Antarctic station is from Lartaud et al. (2010a); from Chapron et al., 2020 for the Lacaze-Duthiers Canyon; from McClanahan et al. (2007) for Tiwi Beach (Kenya) (mean of measurements performed in 1982–1983, 1987–1988 and 1997–1998) and from Huyghe et al. (2019) for the Baie des Veys. For *Magallana gigas*, the periods corresponding to the winter (blue lines) and summer (red lines) samplings are reported. For oysters of the Baie des Veys, a picture of the hinge area observed under cathodoluminescence with the illustration of the Mn^{2+} chemical markings that allow illustrate for an attribution of an absolute age to each sampling is reported. The same has been done for oysters from Tes.

−1.8 ± 0.3 °C, with short-term temperatures ranging between −2.1 °C and brief seasonal warming peaks around −0.5 °C between January and March due to warmer freshwater input (Fig. 2; Lartaud et al., 2010a). Seawater oxygen-isotope ($\delta^{18}O_w$) measurements from 15 km to the NE of the sampling site yield a mean value of −0.2 ± 0.2‰ (1SD) relative to VSMOW (Srivastava et al., 2007; https://data.giss.nasa.gov/o18data). *In situ* calcein markings of different specimens from the same site revealed slow but uninterrupted shell growth with fortnight related growth increments (Lartaud et al. 2010a).

2.2. Neopycnodonte cochlear

Five specimens of the deep-sea oyster species *Neopycnodonte cochlear* were collected in March 2010 at 270 m depth in the Lacaze-Duthiers canyon, in the NW Mediterranean Sea, ~20 km east from the French coast offshore of Banyuls-sur-mer (Fig. 1E; 42°32.10 N, 03°27.19E). Except for brief (i.e., hours to days), very occasional temperature drops of ~ 1 °C due to downwelling currents, mean local temperature remained constant at 13.44 ± 0.10 °C (1SE), as did salinity at 38.52 ± 0.04 psu (Fig. 2Durrieu de Madron et al., 2013; Chapron et al., 2020).

In order to constrain the oxygen-isotope composition of seawater at the site where the five *N. cochlear* were collected in the Mediterranean Sea, twenty-two water samples of 20 mL each were collected *in situ*. They were stored at low temperature to avoid fractionation effects caused by evaporation. Analyses were performed at the Institut d'Ecologie et des Sciences de l'Environnement de Paris at Grignon by CO_2-H_2O equilibration (Epstein and Mayeda, 1953) using an isotope ratio mass spectrometer coupled to an Aquaprep (Isoprime coupled to a Gilson X222, Micromass; analytical reproductibility: 0.15‰). Values oscillate between 0.28 and 0.93‰ relative to VSMOW, with an annual average value of 0.7 ± 0.2‰ (1SE, Supplementary material 1).

No precise calibration of growth for *N. cochlear* exists yet, but the congeneric species *N. zibrowii* has been shown to be a very long-lived species (i.e., reaching > 500 years old) with low growth rates (Wisshak et al., 2009), and one may expect *N. cochlear* to have similarly slow calcification rates.

2.3. Magallana gigas

The oysters of the species *Magallana gigas* (former *Crassostrea gigas*, Salvi and Mariottini, 2017) analyzed in this study are from *in situ* experiments conducted in two farming sites on French coasts, one in the English Channel (Normandy, Baie des Veys) and the other on the Atlantic coast, (Arcachon Basin, Tes) (Fig. 1B-D). Environmental conditions including seawater temperature and salinity were recorded every 15 min during the whole growth period using a YSI multi-parameter probe directly attached to the oyster tables (Fig. 2Lartaud et al., 2010b; Huyghe et al., 2019).

We selected oysters bred between January 2005 and November 2006 in the Baie des Veys (samples labelled BDV) and between January 2005 and September 2006 in the Arcachon basin (samples labelled TES). Collecting seasonal samples for clumped-isotope analyses, required a precise, independent age model. Mn^{2+} chemical markings of the shells were thus performed quasi-monthly during the whole growing experiment period (Huyghe et al., 2019). This Mn-based age model was demonstrated to align well with high resolution $\delta^{18}O$ on other shells from the same site (Huyghe et al., 2020), which gives confidence in applying it to other shells from the same place. To this aim, oysters were immerged during 4 hours in a tank filled with seawater containing 90 mg L^{-1} of manganese chloride tetrahydeate ($MnCl_2$ $4H_2O$), following the protocol of Lartaud et al. (2010b). Before collecting samples for isotopic analyses, the hinge area of each specimen was observed under cathodoluminescence (CL) microscopy to precisely locate the chemical markings, Mn^{2+} being an activator of luminescence (Fig. 2). Absolute dates were attributed to each Mn^{2+} marking identified within the hinge, allowing precise microsampling of specific time intervals (summer and winter) within this area, with reliable correspondence between environmental parameters and the collected samples (Fig. 2; see Lartaud et al., 2010b; Huyghe et al., 2019 for more details about age model construction).

At the BDV site, $\delta^{18}O_w$ values were measured monthly and also reconstructed at sub-daily time scales based on salinity measurements according to the equation of Lartaud et al. (2010c). These $\delta^{18}O_w$ values range between −0.33 and 0.13‰ relative to VSMOW (-0.09‰ on average, Huyghe et al., 2020). At the TES site, $\delta^{18}O_w$ was reconstructed from weekly local salinity measurements, also according to the equation of Lartaud et al. (2010c).

Five BDV specimens were collected in November 2006. At this site, seawater temperatures display seasonal, quasi-sinusoidal fluctuations with minimum and maximum values of 5 °C from January to March and 20 °C from July to September, respectively, whereas salinity remained almost constant throughout the year at ~ 33–34 psu (Fig. 2Huyghe et al., 2019). Three time intervals were targeted for isotopic measurements. The first one ranged from January to the end of February 2005, during the juvenile period (<1 year) of the life of these oysters. The second and third intervals, corresponding to oyster "adulthood", were associated to November 2005 to March 2006 (i.e., winter period) and to July to September 2006 (i.e. summer period), respectively (Fig. 2). During the sampled winter intervals, seawater temperature ranged between 5.9 and 8.9 °C (mean = 7.5, SD = 0.9 °C) in 2005 and between 5.3 and 13.4 °C (8 ± 0.4 °C) in 2006, whereas summer temperature ranged between 16.3 and 20 °C (18.7 ± 0.2 °C).

Four oysters were sampled at TES in September 2006. During the studied period, temperature fluctuated between 4.2 and 26.5 °C and salinity between 24.9 and 34.9 psu. Here, the two sub-sampled intervals extended from December 2005 to February 2006 (winter), and from June to September 2006 (summer), with temperatures ranging from 4.2 to 9.9 °C (7.4 ± 1.3 °C) and between 19.4 and 26.5 °C (22.5 ± 2.1 °C) respectively. We did not sample the juvenile interval for these oysters as these specimens had very little thickness of foliated calcite, which restricted the carbonate material available for precise clumped-isotope analysis.

2.4. Saccostrea cucullata

The "warm" end-member specimens analyzed here are from Tiwi Beach, on the Kenyan coast of the Indian Ocean (4°14.316'S, 39°36.218'E). Four *S. cucullata* oysters were collected from shallow intertidal waters in September 2005. In this area, monthly means of open seawater temperature vary from 25.1 to 28.5 °C between August and February, with an annual mean of 26.8 ± 0.85 °C (1SE) (Fig. 2McClanahan et al., 2007). Neither salinity nor $\delta^{18}O_w$ observations are readily available for this site. The shell growth model reported by Arkhipkin et al. (2017) based on *S. cucullata* from the tropical Atlantic, is characterized by slower growth rates than the temperate *M. gigas* species (Lartaud et al., 2010b), but we still lack a precise shell growth calibration for specimens from the Indian ocean.

3. METHODS

3.1. Sample preparation and sampling

Once specimens were collected, soft tissues were manually removed from the shells, which were then cleaned using de-ionized water. Organic matter was removed by soaking in 5% H_2O_2 for 6 hours according to the protocol of Lartaud et al. (2010c).

Different sampling strategies were used, depending on mollusk species. The most classical way is sampling in the outer shell layer from the hinge to the ventral margin. This was the approach adopted for *A. colbecki*, which lives in seawater with a constant temperature (Fig. 2) by breaking off a 10-mm-long piece of the shell and ground it in an agate mortar. For oysters (*M. gigas*, *S. cuculata* and *N. cochlear*), calcite samples were collected from the hinge area, which comprises both the complete ontogenetic record of oysters and the record of environmental conditions experienced throughout their life (Lartaud, et al., 2010b). As opposed to most other bivalve studies, oyster studies often target the hinge area instead of the whole shell section, providing a condensed growth record on a small shell area, which is usually less impacted by algal deposits and shell boring species (Langlet et al., 2006; Lartaud et al., 2010c). Moreover, because the hinge portion located under the ligamental area has a homogeneous microstructure of foliated calcite (Carter, 1980) it is more resistant to diagenetic alteration than the rest of the shell (Lartaud et al., 2006). We collected "bulk" hinge samples from *N. cochlear* and *S. cucullata*, which live in environments where temperature exhibit no or few seasonal variations (Fig. 2). For *M. gigas*, we micro-sampled with a Dremel the "summer", "winter", and (in the case of BDV specimens) "juvenile" time intervals identified from the Mn^{2+} markings (Fig. 2) using cathodoluminescence observations.

3.2. Clumped isotope analyses

A total of 178 clumped-isotope analyses, comprising 109 shell analyses and 69 carbonate standard measurements, were performed over three analytical sessions in late 2017 and early 2018 at the Laboratoire des Sciences du Climat et de l'Environnement (LSCE), using the equipment and protocols described by Peral et al. (2018) and Daëron et al. (2019) (Supplementary data 1). In each analysis, 2.0–2.3 mg of carbonate powder were dissolved for 15 minutes in a common phosphoric acid bath at 90 °C. Water was then cryogenically removed and the evolved CO_2 passed through a Porapak Q column (50/80 mesh, 1 m length, 2.1 mm ID) held at −20 °C under helium 6.0 flow (25 mL/min). CO_2 was then quantitatively recollected by cryogenic trapping, and transferred by gas expansion into an Isoprime 100 dual-inlet isotope ratio mass spectrometer equipped with six Faraday collectors (m/z 44 to 49). Each sample was analyzed for ~ 3 hours during which analyte and working reference gases were allowed to flow from matching, 10 mL reservoirs into the source through a pair of fused silica capillaries (65 cm length, 110 μm ID). Every 20 minutes, gas pressures were adjusted to achieve a mass 44 current of 40nA, with differences between sample and reference gas generally below 0.1nA. Background currents were measured in all high-gain collectors (m/z 45 to 49) before and after each pressure adjustment, with gas flowing into the source, and are found to be strongly correlated with mass 44 current.

Background-corrected ion current values were processed using the IUPAC isotopic parameters (Brand et al., 2010) to compute $\delta^{13}C_{VPDB}$, $\delta^{18}O_{VPDB}$ and Δ_{47raw} values for each analyte. The single-isotope composition ($\delta^{13}C$, $\delta^{18}O$) of our working reference CO_2 was computed based on nominal $\delta^{13}C_{VPDB}$, $\delta^{18}O_{VPDB}$ values reported by Bernasconi et al. (2018) for carbonate standards ETH-1, ETH-2, and ETH-3, and an oxygen-18 acid fractionation factor of 1.00813 (Kim et al., 2007). "Absolute" Δ_{47} values were computed from Δ_{47raw} by comparison to carbonate standards ETH-1 to ETH-3 using the "pooled" standardization approach of Daëron (2021) and are normalized to the InterCarb Carbon Dioxide Equilibrium Scale (I-CDES, Bernasconi et al., 2021). All data processing was performed using the open-source *D47crunch* library (Daëron, 2021), and all analytical uncertainties reported here are based on the long-term repeatability of Δ_{47} measurements and fully account for the effects of standardization. The long-term repeatability of Δ_{47} values was 15.4 ppm for the three carbonate standards (n = 69, Nf (Number of degrees of freedom) = 60), and 13.8 ppm when taking all analyses into account (n = 194, Nf = 148). The long-term external reproducibilities of $\delta^{13}C_{VPDB}$ and $\delta^{18}O_{VPDB}$ measurements on the carbonate standards were 0.04‰ and 0.09‰, respectively.

3.3. Temperature estimates from $\delta^{18}O$

All carbonate clumped isotope measurements also yield $\delta^{18}O$ and $\delta^{13}C$ values. As a potential strategy to constrain the mineralization temperatures of our bivalves (except *S. cucullata,* for which water composition constraints were insufficient), we computed temperature estimates using traditional oxygen-18 methods. For *N. cochlear* and *M. gigas* from the BDV we used directly measured $\delta^{18}O_w$ values, and

Table 1
All bivalve samples analyzed in the present study, listed by locality, specimen, and shell growth period, and sorted into eight groups by calcification temperature. Temperature estimates preceded by an asterisk are based on oxygen-18 fractionation between shell calcite and local water (Eq. (1)), to account for warm-biased calcification rates and potential subsampling imprecision (see Section 5.1). All other temperature estimates are based on *in situ* temperature records. Sample group averages of Δ_{47} are computed using the D47crunch library to account for covariance in analytical errors (Daëron, 2021).

Locality	**Lattitude**	**Longitude**	**Depth (m)**	**Species**	**Time interval**	**Specimen**	**Sample**	**Replicate analyses**	**δ13C (‰ VPDB)**	**δ^{18}O (‰ VPDB)**	**Δ47 I-CDES (‰ ±95%)**	**Sample group**	**δ^{18}O (‰, VSMOW)**	**Salinity (psu)**	**Instrumentallymeasured Temperature (°C ± 1SD)**	**Temperature from δ^{18}O (°C)**	**Δ47 I-CDES (‰ ±95%)**
Dumont d'Urville station (Antarctica)	−66.657667°	140.008333°	15	*A. colbecki*		Ad1	Ad1	4	2.10	4.66	0.6803 ± 0.0165	Ad	0.2 ± 0.2	-	−1.80 ± 0.50	−1.88	0.6893 ± 0.0119
						Ad3a	Ad3a	4	1.99	4.68	0.6933 ± 0.0166						
						Ad3l	Ad3l	4	1.97	4.67	0.6944 ± 0.0166						
Lacaze- Duthiers canyon (France)	42.545556°	3.420833°	270	*N. cochlear*		PY1	PY1	4	0.51	2.82	0.6444 ± 0.0160	PY	-	38.52 ± 0.04	13.44 ± 0.1	7.99	0.6397 ± 0.0097
						PY2	PY2	4	0.64	2.64	0.6434 ± 0.0160						
						PY3	PY3	4	0.99	2.55	0.6353 ± 0.0159						
						PY4	PY4	4	1.13	2.59	0.6252 ± 0.0159						
						PY5	PY5	4	0.84	2.44	0.6500 ± 0.0160						
Tiwi Beach (Kenya)	−4.238596°	39.603634°	0	*S. cucullata*		TW1	TW1	5	1.53	−0.63	0.5863 ± 0.0142	TW	-	-	26.80 ± 0.85	-	0.6001 ± 0.0095
						TW2	TW2	4	0.51	−0.98	0.5993 ± 0.0156						
						TW3	TW3	4	1.11	−0.87	0.6090 ± 0.0156						
						TW4	TW4	4	1.21	−0.77	0.6092 ± 0.0156						
Baie des Veys (France)	49.385167°	−1.100833°	0	*M. gigas*	Juvenile	BDV-3	BDV-3 J	2	−0.36	−0.87	0.6209 ± 0.0201	BDV-J	−0.25 ± 0.21	32.04 ± 0.94	7.50 ± 0.90	17.25	0.6258 ± 0.0143
						BDV-5 + BDV-7	BDV-5J7J	1	−0.04	−0.05	0.6284 ± 0.0272						
						BDV-6	BDV-6 J	1	−0.51	0.05	0.6096 ± 0.0271						
						BDV-6 + BDV-7	BDV-6J7J	1	−0.53	0.24	0.6492 ± 0.0274						
					Summer	BDV-2	BDV-2S	4	−0.77	−0.83	0.6092 ± 0.0154	BDV-S	0.15 ± 0.08	33.4 ± 0.38	18.70 ± 0.75	19.73	0.6121 ± 0.0097
						BDV-3	BDV-3S	4	−0.73	−0.82	0.6019 ± 0.0153						
						BDV-5	BDV-5S	4	−1.31	−0.73	0.6118 ± 0.0154						
						BDV-6	BDV-6S	4	−1.21	−0.64	0.6210 ± 0.0149						
						BDV-7	BDV-7S	4	−1.30	−0.84	0.6165 ± 0.0155						
					Winter	BDV-2	BDV-2 W	4	−0.88	0.97	0.6409 ± 0.0157	BDV-W	0.2 ± 0.05	33.9 ± 0.25	*11.01 ± 1.00	11.01	0.6349 ± 0.0103
						BDV-3	BDV-3 W	4	−1.22	1.40	0.6335 ± 0.0156						
						BDV-5	BDV-5 W	4	−1.24	1.11	0.6362 ± 0.0156						
						BDV-6	BDV-6 W	4	−1.34	1.13	0.6451 ± 0.0157						
						BDV-7	BDV-7 W	4	−1.50	0.69	0.6187 ± 0.0154						
Arcachon Basin (France)	44.666833°	−1.136333°	0	*M. gigas*	Summer	TES-13	TES-13S	2	−0.46	−1.33	0.6030 ± 0.0200	TES-S	0.06 ± 0.21	33.47 ± 0.96	22.50 ± 2.10	21.66	0.5972 ± 0.0105
						TES-2	TES-2S	5	−1.07	−1.13	0.5875 ± 0.0132						
						TES-3	TES-3S	4	−0.86	−1.28	0.6065 ± 0.0153						
					Winter	TES-2 + TES-3	TES-2W3W	1	−0.87	0.11	0.6343 ± 0.0273	TES-W	−0.67 ± 0.5	30.15 ± 2.28	*12.23 ± 1.00	13.6	0.6329 ± 0.0202
						TES-4	TES-4 W	1	−0.39	0.38	0.6315 ± 0.0272						

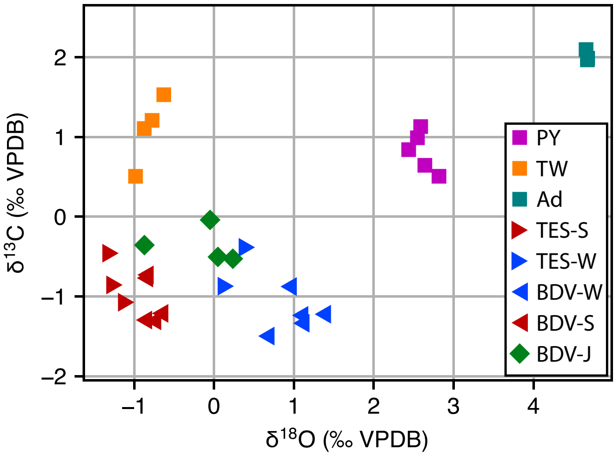

Fig. 3. Average $\delta^{18}O$ and $\delta^{13}C$ values of all specimens analyzed in this study. Each marker corresponds to the unweighted average of all measurements performed on a single bivalve sample as part of the clumped-isotope analyses. Corresponding values are listed in Table 1. PY = *Neopycnodonte cochlear*; Ad = *Adamussium colbecki*; BDV-J = *Magallana gigas* from Baie des Veys, juvenile period; BDV-W = *Magallana gigas* from Baie des Veys, winter period; BDV-S = *Magallana gigas* from Baie des Veys, France, summer period; TES-W = *Magallana gigas* from Tes, winter period; TES-S = *Magallana gigas* from Tes, summer period; TW = *Saccostrea cucullata*.

for *A. colbecki* water composition was estimated from the Global Seawater Oxygen-18 Database of LeGrande and Schmidt (2006). For TES, $\delta^{18}O_w$ was calculated using salinity measurements using the equation of Lartaud et al. (2010c). All environmental data are synthetized in Table 1.

To estimate the mineralization temperatures for *M. gigas* and *N. cochlear* oysters and the pectinid species *A. colbecki* we used the synthetic calcite regression of Kim and O'Neil (1997) (Eq. (1), modified for consistency with the use of an acid fractionation factor of 1.01025):

$$T\ (^{\circ}C) = ((18030\ /1000\ln a_{\alpha c-w}) + 32.17) - 273.15 \qquad (1)$$

where $\alpha_{c\text{-}w}$ corresponds to the fractionation coefficient between calcite and water:

$$a_{c-w} = (1000 + d^{18}O_{c\ VPDB}) \times 1.03092\ /(1000 + d^{18}O_{w\ VSMOW}) \qquad (2)$$

where $\delta^{18}O_c$ corresponds to the measured $\delta^{18}O$ of calcite relative to VPDB and $\delta^{18}O_w$ to the $\delta^{18}O$ of the seawater relative to VSMOW.

For the pectinid species *A. colbecki*, we compared these Kim & O'Neil estimates to those obtained from the equation of Chauvaud et al. (2005) established for calcite material of pectinid species from the French Atlantic coast:

$$T\ (^{\circ}C) = 14.84 - 3.75\ (\delta^{18}O_{CVPDB} - \delta^{18}O_{sw\ VSMOW}) \qquad (3)$$

4. RESULTS

4.1. $\delta^{18}O$ and $\delta^{13}C$

We show in Fig. 3 the average $\delta^{18}O$ and $\delta^{13}C$ values for all 31 clumped-isotope samples. Each value reported here corresponds to the mean of one to five analyses performed on one individual shell (cf Table 1), depending on the amount of carbonate available. Each sample group exhibits low $\delta^{18}O$ variability (from 0.1 to 0.7‰) compared to the variability in $\delta^{13}C$ values (from 0.2 to 1‰) except for sample BDV-J. Antarctic *A. colbecki* samples yield the greatest $\delta^{18}O$ values (mean = 4.45‰, SD = 0.06‰), followed by deep-sea Mediterranean *N. cochlear* (2.45‰, SD = 0.13‰). By contrast, temperate and tropical oysters yield the lowest values. *M. gigas* shells from BDV have a mean value of −0.78‰ (SD = 0.10‰) during the summer period whereas shells from TES have a mean value of −1.25‰ (SD = 0.15‰) during this season. The Kenyan oysters (*S. cucullata*) have an annual average value of −0.85‰ (SD = 0.16‰). The $\delta^{18}O$ of *M. gigas* shells in winter are slightly greater, and more variable than for other samples, with 1.02‰ (SD = 0.25‰) for BDV-W, −0.34‰ (SD = 0.5‰) for sample BDV-J and 0.02‰ (SD = 0.24‰) for TES-W.

Regarding carbon-13, *A. colbecki* yields the highest values and lowest variability (2.00 ± 0.06‰, 1SD). *Saccostrea cucullata* and *N. cochlear* have intermediate values of 1.11 ± 0.38‰ and 0.83 ± 0.23‰ respectively. Oysters of the species *M. gigas* have the lowest values. In the BDV, these oysters have $\delta^{13}C$ values of −1.02 ± 0.26‰ during summer, −0.33 ± 0.19‰ during the first winter (i.e. during the juvenile phase, BDV-J) and −1.19 ± 0.21‰ during the second winter (BDV-W). In Tes, oysters exhibit $\delta^{13}C$ of −0.85 ± 0.23‰ during summer and −0.53 ± 0.21‰ during winter.

4.2. Clumped isotopes

Clumped-isotope compositions of mollusk shells are summarized in Table 1 and fully reported in research data 1. Sample-averaged Δ_{47} values range between 0.6 and

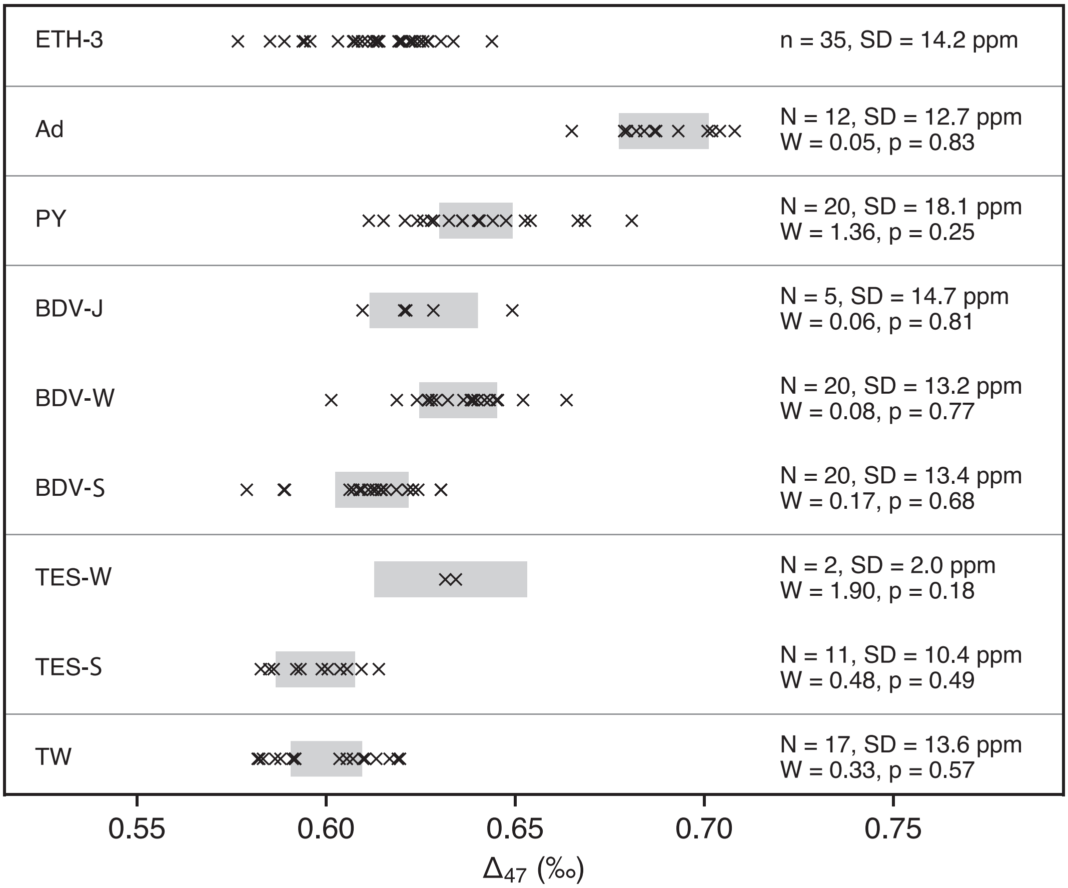

Fig. 4. Δ_{47} values for all replicate analyses of bivalve samples, binned by sample group (cf Table 1). A Levene test of heteroscedasticity was used to check whether the observed Δ_{47} variability among each group differs significantly from that for the standard ETH-3 (top row). N: total number of analyses within each group; SD: sample standard deviation of Δ_{47} analyses within each group; W: Levene's test statistic; p: *p*-value for the null hypothesis that the underlying population variance within each group is equal to that within all ETH-3 analyses. All sample groups analyzed here display no more internal Δ_{47} variability than expected from analytical repeatability alone.

0.7‰ (I-CDES). One of the samples, TES-13 W, corresponding to winter calcification of the *M. gigas* specimen TES-13, could only be analyzed twice and yielded two very different Δ_{47} values of 0.574 and 0.614‰ much further apart than expected from our usual analytical repeatability (see supplemental data 1). Although we found no obvious technical problem with the two corresponding measurements, it is possible (yet conjectural) that we mis-identified growth sections exclusively associated with winter in this specimen, which could explain the relatively low Δ_{47} values for this sample (but not its apparent isotopic heterogeneity). For lack of a better option, we opted to discard the results obtained for sample TES-13 W, leaving only two other winter specimens from this locality.

Although each sample was subjected to relatively few analyses (four replicates when possible, but fewer for juvenile oysters and most samples from Arcachon), the total number of replicate analyses corresponding to a given calcification temperature is generally much larger (up to 20). As a result, it may be possible to constrain more precisely Δ_{47} values associated with each calcification temperature by binning together samples formed in the same environmental conditions ("Sample groups in Table 1"). Such binning of samples, however, rests on the implicit assumption that the scatter in our Δ_{47} results mostly reflects analytical uncertainties rather than true heterogeneities between specimens and/or environmental variability, which is consistent with the low variability of $\delta^{18}O$ within each sample group. To test this assumption, we subjected the sample distribution of Δ_{47} values for each temperature group to a Levene test designed to assess whether the scatter in any group is significantly larger than expected based on the entire sample distribution of Δ_{47} values for the ETH-3 standard (N = 35). As shown in Fig. 4, all groups yield p-values consistent with the null hypothesis (equal variances), implying that the observed scatter primarily reflects random

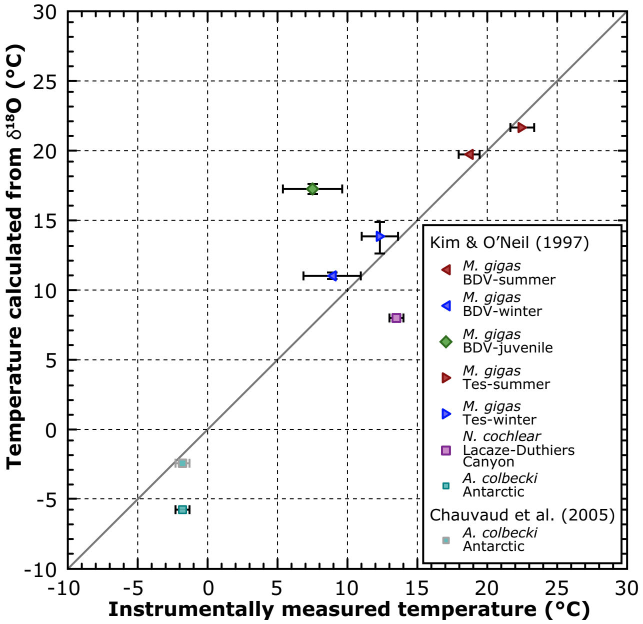

Fig. 5. Comparison between the temperatures instrumentally measured in the sampling sites and the temperatures calculated from the $\delta^{18}O$ values and the equation of Kim and O'Neil (1997). The equation of Chauvaud et al. (2005) was also tested for the pectens (*Adamussium colbecki*, green diamonds). Each point represents a mean of all samples from a given sample group, as defined in Table 1. A 1 : 1 line is reported on the graph.

analytical uncertainties. Thus, in the forthcoming discussion, we compare each of the eight calcification temperatures listed in Table 1 to the corresponding average Δ_{47} values (weighted by number of analyses) for each sample group, computed using the D47crunch library to account for analytical error covariances (Daëron, 2021).

5. DISCUSSION

Here, we attempt to address three core issues. First, as a prerequisite to the rest of the discussion, how (and how precisely) can we obtain optimal constraints, independently of the clumped-isotope measurements, on the calcification temperatures of our samples? Next, does Δ_{47} in our samples vary systematically as a function of temperature alone, or do we find evidence for clumped-isotope disequilibria? Finally, how do our bivalve observations compare with earlier results, whether or not they predate the I-CDES reference frame?

5.1. *Independent constraints on calcification temperatures from* in situ *observations and/or oxygen-18 thermometry*

In the case of the tropical oyster *S. cucullata,* we are unable to compare *in situ* temperature observations to oxygen-18-derived estimates because neither salinity nor $\delta^{18}O_w$ were monitored at this site. Relying on $\delta^{18}O_w$ values from the GISS database for these samples is also not possible as they come from shallow water environments where the evaporation/precipitation ratio fluctuates strongly over the year, as well as freshwater input from land. However, these specimens are from reduced seasonality environments (~3 °C annual amplitude), so that the environmental temperature constraints are sufficient for our purpose.

For all the other samples, Fig. 5 provides a comparison between directly measured seawater temperatures and temperatures calculated from Eqs. (1)–(3). We find good agreement for both summer *M. gigas* sample groups (BDV-S and TES-S). On the contrary, juvenile / winter *M. gigas* (BDJ-J, BDV-W, and TES-W) yield discrepancies up to 10 °C between the two temperature estimates. Although many previous works have found that oysters mineralize their shells following a systematic relationship between carbonate/water oxygen-18 fractionation and calcification temperature (Wefer and Berger, 1991; Kirby et al., 1998; Surge et al. 2001; Ullmann et al. 2010; Tynan et al. 2014), several works showed that minimum winter temperatures are not always recorded and/or difficult to sample reliably due to very slow calcification rates likely reflecting a combination of cold temperatures and reduced food (Lartaud et al., 2010b, c; Ullmann et al., 2010; Huyghe et al., 2019). In BDV and TES winter settings, growth rate tends to increase with environmental temperature, making calcification-weighted average temperatures for winter periods significantly warmer than time-weighted average environmental temperatures (Fig. 2Huyghe et al., 2019). It is also possible, due to the large amount of carbonate required for clumped isotopes (2.0–2.3 mg per analysis), that we unknowingly sampled small amounts of carbonate mineralized during early spring or late fall, which might explain the higher inter-specimen variability of $\delta^{18}O$ values for winter samples relative to summer ones (Fig. 3). As a result of these two issues, oxygen-18 thermometry likely provides more accurate estimates of calcification temperatures for non-juvenile winter *M. gigas* samples, and in the rest of this study we use these ^{18}O-derived estimates as independent temperature constraints for sample groups BDV-W and TES-W. It should be noted that this approach yields larger temperature uncertainties for the latter, due to the fact that salinity (and thus $\delta^{18}O_w$) values remained stable throughout the year at Baie des Veys (Fig. 2), whereas seasonal variations are much larger for TES-W.

Juvenile *M. gigas* samples yield even greater discrepancies, with Kim & O'Neil - derived temperatures warmer by ~ 10 °C than *in-situ* seawater measurements for this period, and also than ^{18}O-derived temperatures for the following winter with similar environmental temperatures. Studies based on specimens from the same site (Huyghe et al., 2019, 2020) recently observed very rapid growth rates during this early stage of the oysters' lives (Fig. 2), along with anomalous oxygen-18 fractionation up to 3‰ relative to Kim & O'Neil (1997). This discrepancy (BDV-J vs BDV-W) among oysters of the same spat is too large to result only from subsampling interval errors, and we conclude instead that they reflect ontogenic effects associated with this juvenile development stage (Huyghe et al., 2020), as already documented in other mollusks (McConnaughey, 1989; Mitchell et al., 1994). In the forthcoming discussion, we must thus tentatively rely on the *in situ* observations to constrain calcification temperature.

Temperatures derived from Kim and O'Neil (1997) for the deep-sea oysters (*N. cochlear*) are 5 °C colder than direct measurements despite quasi-constant environmental conditions (Fig. 2). Such disequilibrium towards higher δ^{18}O values is surprising compared to classical models driven by kinetic effects or thermodynamic response to biologically induced pH gradient in the calcifying region that lead ^{18}O depleted carbonates (Adkins et al., 2003). But this observation is qualitatively consistent with earlier findings concerning another *Pycnodonte* species, where Wisshak et al. (2009) observed an average oxygen-18 enrichment of 0.5‰, relative to Kim and O'Neil (1997) in giant deep-sea oysters *Neopycnodonte zibrowii* from the northeastern Atlantic. A positive deviation of ~ 1‰ compared to isotopic equilibria was also reported from coastal barnacle and gastropod shells (Killingley and Newman, 1982; Fenger et al., 2007) without clear explanation yet. These biological fractionation processes could be more common than presently though, and might be more easily identifiable in deep sea settings where environmental variables are usually more stable than in coastal shallow ecosystems.

Oxygen-18-based estimates of calcification temperature for our *A. colbecki* samples suffer from the fact that the potential ^{18}O equations of Kim and O'Neil (1997) and Chauvaud et al. (2005) are both calibrated with minimum temperatures of 10 °C (compared to −2 °C in this study), leading to potentially large extrapolation biases. Our own measurements yield calcite δ^{18}O values 1.04‰ and 0.21‰ higher than predicted, respectively, from Eqs. (1) and (3). At any rate, because of quasi-constant environmental conditions at this locality, oxygen-18 thermometry is unlikely to provide better constraints on calcification temperatures than the existing *in situ* observations (−1.8 ± 0.5 °C, 1SD).

Based on all the above arguments, Table 1 lists our best estimates of calcification temperature for all sample groups.

5.2. Relationship between clumped isotopes and calcification temperature

Fig. 6 plots the average Δ_{47} values, weighted by number of analyses, for each sample group against the corresponding estimates of growth temperatures. Low-seasonality samples Ad, PY, TW and both summer-precipitated *M. gigas* samples BDV-S and TES-S yield Δ_{47} values which are strongly correlated with temperature. This holds true as well for adult winter *M. gigas* samples (BDV-W, TES-W) in spite of large analytical uncertainties on the latter. A York regression (York et al., 2004) taking into account all samples except BDV-J yields the following relationship between calcification temperature (T, in K) and Δ_{47} (in‰, I-CDES):

$$\Delta_{47} = 38.01 \times 10^3 / T^2 + 0.171 \tag{4}$$

The reduced χ^2 statistic for this regression is equal to 1.3 for 5 degrees of freedom, implying that the combined uncertainties affecting analytical errors and calcification temperature estimates are sufficient ($p = 0.26$) to explain the observed regression residuals. Regression uncertainties are best expressed by reformulating Eq. (4) as below, where T_0 is chosen so that model errors in slope and intercept values are statistically independent:

$$\Delta_{47} = A \times 10^3 \, (1/T^2 - 1/T_0^2) + B$$
$$A = 38.01 \pm 3.56 \text{ (1SE)}$$
$$B = 0.629 \pm 0.003 \text{ (1SE)}$$
$$T_0 = 15.0 \text{ K}$$

By contrast with all the other samples, the juvenile *M. gigas* samples plot well outside of the confidence region for the above regression. This is perhaps not surprising in view of the strong ontogenic biases affecting oxygen-18 observed above (see also Huyghe et al., 2020), but could also conceivably reflect the fact that the constraints on BDV-J calcification temperature are from *in situ* temperature records, instead of oxygen-18-derived estimates as for the other two winter samples (BDV-W, TES-W). We thus test the hypothesis that the apparent offset of BDV-J could results from a thermal "warm bias" in calcification rates causing most shell to precipitate in the warmest periods by comparing, in Fig. 7, the daily distribution of true seawater temperatures to the apparent temperatures derived either from oxygen-18 or from Δ_{47}, for all three BDV sample groups. We find that both isotopic temperature estimates for the juvenile group are much warmer than the warmest local conditions on record, even considering their full 95% confidence regions. By contrast, both isotopic estimates for the BDV-W and BDV-S are consistent with the upper range of temperatures recorded *in situ*. We conclude that the observed offset between BDV-J and the regression line in Fig. 6 cannot result from thermal bias alone.

As shown in Fig. 8, the isotopic disequilibria manifested by BDV-J seem consistent at first glance with those pre-

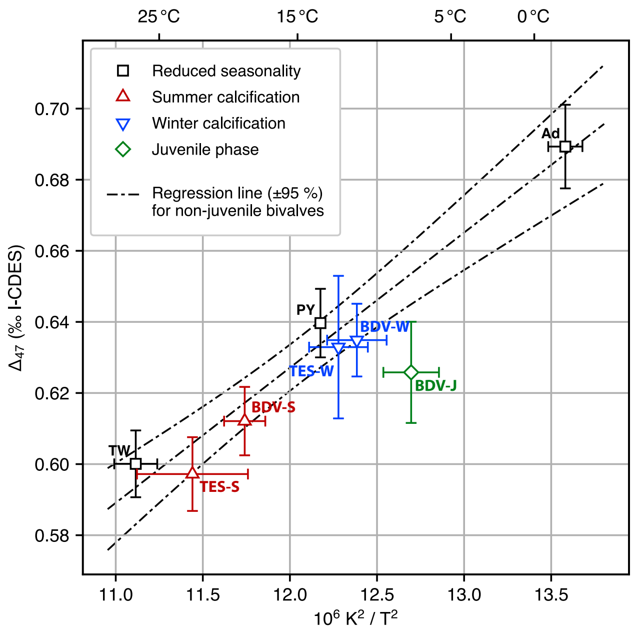

Fig. 6. Mean Δ_{47} values as a function of calcification temperature estimates for each sample group (cf. Section 5.1; Table 1). These two parameters are strongly correlated for all sample groups except for juvenile *M. gigas* samples (BDV-J), which yield anomalously low Δ_{47} values.

dicted for DIC speciation effects by Hill et al. (2014), with the observed –2.2‰ offset in $\delta^{18}O$ requiring a calcification pH change of +0.6 or more. It appears unlikely, however, that the differences observed between our juvenile BDV samples and their mature counterparts (both from summer and winter) directly reflect differences in calcification pH, because most of the other factors influencing isotopic fractionations between the calcifying DIC and the mineral phase (crystallization rate, degree of DIC-water equilibration, preferential incorporation of carbonate vs bicarbonate ions…) are also likely to vary greatly between these samples. For instance, Huyghe et al. (2019) showed that typical shell growth rates for BDV-J are ~ 120 µm/day (very roughly equivalent to > 35 µmol/m2/s), but only on the order of 20 µm/day (~6 µmol/m2/s) and 10 µm/day (~3 µmol/m2/s) for BDV-S and BDV-W, respectively. As a result, the juvenile shells are likely to approach kinetic limit fractionations, introducing additional yet poorly constrained fractionations between DIC and the mineral phase (e.g., Watkins and Hunt, 2015, Devriendt et al., 2017).

Conversely, the offsets shown in Fig. 8 first appear to be qualitatively different, with lower than expected values of $\delta^{18}O$ and Δ_{47}, from the well-documented offsets observed, for instance, in corals (lower than expected $\delta^{18}O$ but greater than expected Δ_{47}) and in speleothems (greater than expected $\delta^{18}O$ but lower than expected Δ_{47}). In particular, in deep-sea and surface corals, anti-correlated offsets in $\delta^{18}O$ and Δ_{47} are likely to reflect precipitation from a DIC pool out of isotopic equilibrium with water, due to rapid absorption of CO_2 (Guo, 2020). But the model of Guo is also consistent with negative offsets in both $\delta^{18}O$ and Δ_{47}, as progressive re-equilibration of the DIC produces non-intuitive trajectories in ($\delta^{18}O$, Δ_{47}) space (Fig. 8). The isotopic disequilibria reported here in juvenile *M. gigas* could thus conceivably be controlled by CO_2 absorption kinetics, as is likely the case in corals, despite the apparent discrepancy in ($\delta^{18}O$, Δ_{47}) covariation. Several processes are involved in the mineralization process of molluscan shells. It has been shown that the calcifying matrix is a mixture of different proteins that control the polymorph and the texture of the shell (Marin and Luquet, 2004). Mineralization for mollusks occurs in the extrapallial cavity, that contains a fluid precursor to mineralization that reaches the saturation state. Although it is established that CO_2 absorption is one of several processes involved in bivalve biomineralization, quantitative estimates of this contribution remain elusive. McConnaughey et al. (1997) concluded that metabolic C from respired CO_2 typically accounts for around 10% of mollusk-shell carbonate, yet larger contributions, up to 37%, have been reported in some bivalve species (e.g., Gillikin et al., 2007). The fraction of metabolic C incorporated in the shell is likely to vary greatly between larval, juvenile and mature stages in response to strong differences in mineralization conditions and/or nutrient availability (e.g., Thomsen et al., 2015; Lartaud et al., 2010d).

Testing whether the isotopic offsets of Fig. 8 are driven by differences in calcification pH, in CO_2 absorption kinetics, or by other causes calls for additional, systematic comparisons of juvenile versus mature shell sections in *M. gigas* and other species. For now, juvenile sections of oyster shells (identifiable by sclerochronological or sclerogeochemical approaches in fossils) do not appear to be suitable for isotopic paleotemperature reconstructions.

As illustrated by the good agreement between our *N. cochlear* samples (PY) and the other species studied here, clumped-isotope thermometry potentially provides accurate estimates of temperature even in samples characterized by “anomalous” oxygen-18 fractionation behaviors. It is perhaps significant that our low-seasonality samples (Ad, PY, TW) plot slightly above the regression line of Eq. (4) while the summer and winter *M. gigas* samples plot slightly below. Each of these small positive and negative residuals is well within uncertainties, yet the systematic distribution of samples above and below the line as a function of reduced vs strong seasonality is consistent with warm-biased calcification rates in *M. gigas*, perhaps even in summer samples (cf bottom panel of Fig. 7).

Based on the observations described above, two issues to keep in mind when attempting clumped-isotope reconstructions of paleotemperatures using bivalves are, for one thing, risk that juvenile calcification in *M. gigas* (and potentially in other species from strongly seasonal environments) may exhibit large ^{18}O and Δ_{47} departures from expected values, for reasons yet to be investigated. What is more, shell produced during the winter in strongly seasonal environments must be sampled with caution if there is any indication of reduced growth rates, and it might even then remain impossible to reliably estimate minimum temperatures due to thermal bias in calcification rates.

This issue may likely be mitigated by combining different proxies: as stated above, δ^{18}O in mollusk shells offers high resolution records at sub-seasonal scales but suffer from uncertainties on coeval $\delta^{18}O_w$ values. By contrast, clumped isotopes are independent of $\delta^{18}O_w$ but require comparatively large amounts of carbonate, thus yielding lower-resolution records. Combining Δ_{47} and δ ^{18}O analyses on the same specimens, as recently done in several studies (Van Plantinga and Grossman, 2018; Briard et al., 2020), is a promising approach which should be widely applicable to different periods and environments.

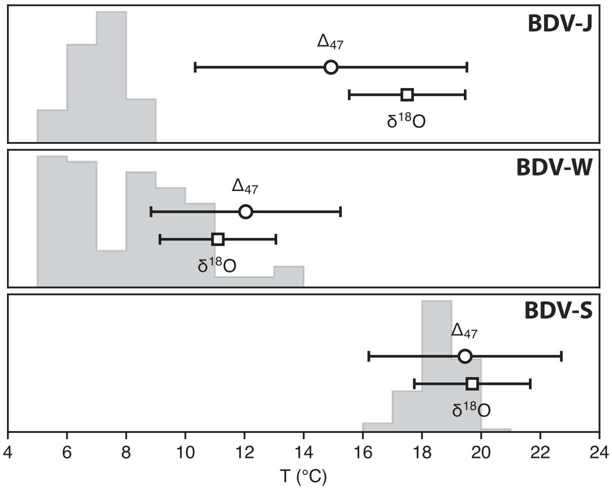

Fig. 7. Comparison, for the three BDV sample groups, of daily *in situ* records of seawater (histograms), apparent calcification temperatures derived from oxygen-18 based on the Kim & O’Neil (1997) equation (square markers with 95% confidence limits) or from clumped isotopes based on the Peral et al. (2018) calibration (round markers with 95% confidence limits), whose applicability to bivalves is illustrated by Fig. 9.

5.3. Comparison with earlier studies and I-CDES calibrations

Our findings are qualitatively consistent with previous studies of clumped isotopes in marine mollusk shells (Eagle et al., 2013; Henkes et al., 2013; Petrizzo et al., 2014), but direct numerical comparisons are not straightforward because of significant methodological differences: (a) the data of Eagle et al. (2013) mostly predate the introduction of an “absolute” Δ_{47} scale referenced to equilibrated CO_2 values (Dennis et al., 2011), and to the best of our knowledge has not been reprocessed using updated ^{17}O correction parameters; (b) there is no strong consensus on which “acid correction” value should be used to compare our measurements to those of Petrizzo et al. (2014), who reacted samples at 25 °C; (c) most importantly, the data reported here were normalized in the I-CDES reference frame, using carbonate standards instead of equilibrated CO_2 gases, and the InterCarb results demonstrate that exclusively relying on gas standards potentially introduces detectable inter-laboratory biases (Bernasconi et al., 2021).

With these caveats in mind, it should nevertheless be safe to compare regression slopes of calibrations even if they were not processed in the same reference frame (Fig. 9). The slope obtained here ($38.01 \pm 3.56 \times 10^3 K^2$, 1SE) is statistically indistinguishable from those obtained from the results of Henkes et al. ($p = 0.16$) and Petrizzo et al. ($p = 0.55$), both reprocessed using the IUPAC ^{17}O correction parameters by Petersen et al. (2019). Our bivalve

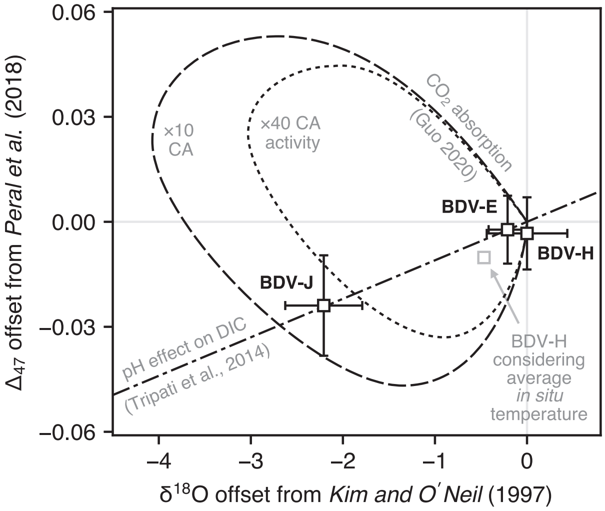

Fig. 8. Isotopic offsets (with 95 % error bars) from expected values observed in the three BDV sample groups. Non-juvenile samples BDV-E and BDV-H yield δ^{18}O and Δ_{47} values consistent with the calibrations of Kim & O’Neil (1997) and Peral et al. (2018), respectively. By contrast, juvenile samples (BDV-J) display lower than expected δ^{18}O and Δ_{47} values, potentially consistent with DIC speciation effects and/or kinetic fractionation effects associated with CO_2 absorption, but not with purely diffusive effects which are expected to decrease δ^{18}O and increase Δ_{47} (Thiagarajan et al., 2011). Note that the choice of Δ_{47} calibration has no bearing on this observation, because Peral et al (2018) is statistically indistinguishable from other I-CDES calibrations (Fig. 9).

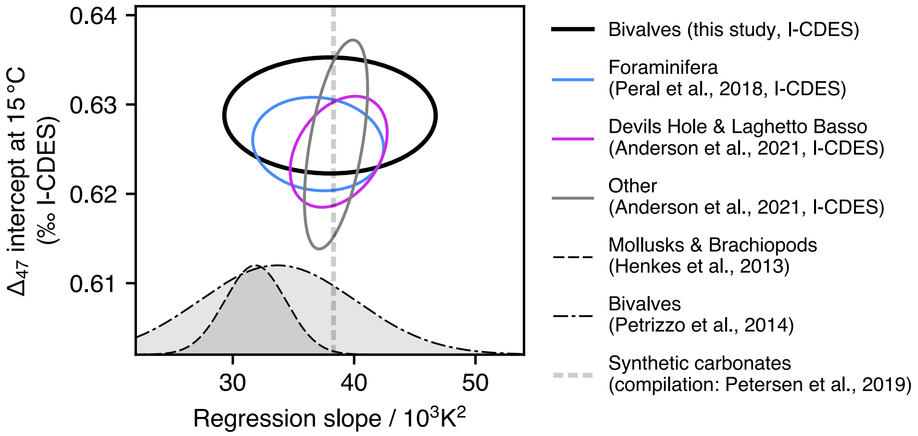

Fig. 9. **(a)** Comparison between our results and those from other calibration studies processed (or reprocessed) in the I-CDES reference frame. There is close agreement between the non-juvenile bivalves analyzed here and Late Holocene foraminifera (Peral et al., 2018), extremely slow-growing calcite from Devils Hole and Laghetto Basso, and various other carbonate materials (Anderson et al., 2021). **(b)** 95% confidence ellipses for the regression slopes and Δ_{47} intercept values at 15 °C for various I-CDES calibrations and the earlier bivalve/mollusk studies of Henkes et al. (2013) and Petrizzo et al. (2014), both reprocessed by Petersen et al. (2019). Because I-CDES and pre-I-CDES Δ_{47} values are not directly comparable, the calibration slopes for Henkes et al. and Petrizzo et al. are only shown as probability distribution functions. For the same reason, only the slope of the composite Petersen et al. (2019) calibration is shown here (dashed vertical line).

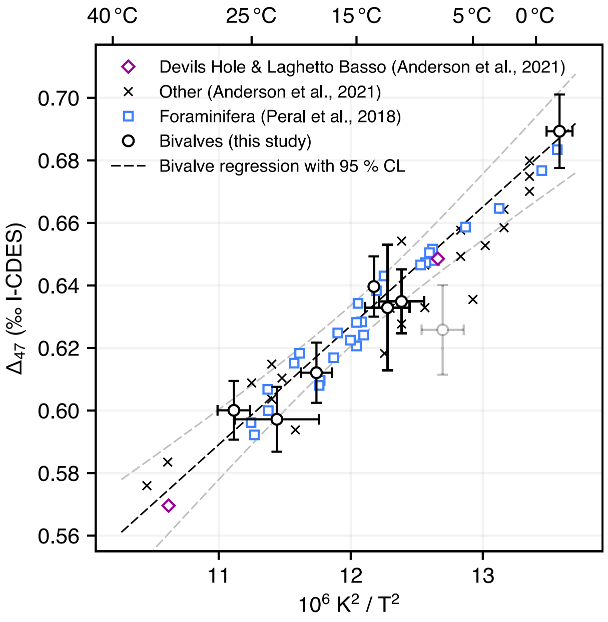

Fig. 10. Comparison between our bivalve regression and that of Peral et al. (2018), which is based on modern/recent benthic and planktonic foraminifera analyzed in the same laboratory, using the same equipment and methods. Results are also compared to the ones of Anderson et al. (2021) and the slow growing calcites of Devils Hole and Laghetto Basso re-analyzed by Anderson et al. (2021).

slope is also virtually identical to that of the combined regression of Petersen et al. (2019).

More quantitatively, Anderson et al. (2021) recently reported I-CDES values for various, mostly inorganic types of carbonates of known formation temperatures, which may be robustly compared to our results. We also reprocessed the original raw data of the foraminifer calibration study of Peral et al. (2018) to convert them to the I-CDES. As shown in Figs. 9 and 10, the bivalve measurements reported here are strictly indistinguishable from the results of these two studies.

It should be noted that Anderson et al. (2021) also report a re-analysis, performed at LSCE, of mammillary calcite from Devils Hole and Laghetto Basso—two carbonate materials with extremely slow growth rates, believed to achieve quasi-equilibrium oxygen-18 fractionation between calcite and water as well as internal clumped-isotope equilibrium—previously described by Daëron et al. (2019, and references therein). Contrary to Daëron et al.'s initial findings, the clumped-isotope composition of Devils Hole calcite reported by Anderson et al. is indistinguishable from the general relationship between Δ_{47} and temperature, as calibrated using carbonates with more rapid growth rates. We believe it likely that the small (0.008‰) but statistically significant Δ_{47} difference initially reported by Daëron et al. (2019) results from the lack of ETH-4 analyses in the 2019 study, causing Devils Hole measurements to plot well outside of the "anchor triangle" of ETH-1/2/3, thus increasing standardization errors (Daëron, 2021).

Whatever the case, the new bivalve data presented here are in complete agreement with the other existing I-CDES calibration studies (Figs. 9 and 10), and thus also with other inorganic and biogenic calibrations (Kele et al., 2015; Piasecki et al., 2019; Meinicke et al., 2020) which have not yet been converted to the I-CDES but are known to be in good agreement with Peral et al. (2018). This observation further supports the claim that various types of "well-behaved" carbonates, either biogenic inorganic, follow quasi-identical relationships between Δ_{47} and formation temperatures (as already proposed by earlier studies, e.g., Came et al., 2014), even in cases of "anomalous" relationships between carbonate/water oxygen-18 fractionation and temperature. Figs. 9 and 10 also illustrate the excellent consistency which may be achieved between I-CDES calibration studies based on sufficiently large numbers of standard and unknown analyses. Based on this, future paleoclimate studies of clumped isotopes in bivalves, rather than relying on the limited number of observations reported here, should not hesitate to use robust, more precise calibrations such as those of Peral et al. (2018) or Anderson et al. (2021).

6. CONCLUSIONS

The observations reported here provide strong support for the use of clumped-isotope thermometry to reconstruct past calcification temperatures from bivalve shells, including at seasonal scale. The confirmation that even species with “anomalous” oxygen-18 fractionation laws (e.g., *N. cochlear)* yield Δ_{47} values indistinguishable from those of other biocarbonates formed at similar temperatures implies that clumped-isotope thermometry may be applicable to well preserved samples from ancient environments with an ocean chemistry quite different from today’s (and thus with potentially different degrees of oxygen-18 disequilibrium).

The excellent agreement between our results and recent calibrations studies (re)processed in the I-CDES reference frame strengthens the case that the systematic use of carbonate standards yields reproducible results between laboratories, even when using different analytical methods (acid temperature, sample size...), as argued by Bernasconi et al. (2021). This agreement also adds to the growing body of evidence that there exists a whole class of carbonate materials, both inorganic and biogenic, characterized by quasi-identical relationships between formation temperature and clumped-isotope composition.

Our findings, however, also highlight the challenges posed by the use of shells whose isotopic composition might behave anomalously during juvenile stages and/or under conditions of thermal and/or metabolic stress. As always, fossil sampling strategies, e.g., when trying to constrain past seasonal variations of temperature, should build on a robust understanding of the biology, ecology, and geochemistry of the target species.

Declaration of Competing Interest

The authors declare that they have no known competing financial interests or personal relationships that could have appeared to influence the work reported in this paper.

ACKNOWLEDGEMENTS

This project was financially supported by the ANR AMOR (Data Model Reconstruction of the Cenozoic Climate). The authors thank Laurent Chauvaud and Erwan Amice (LEMAR, UBO) for the collection of *A. colbecki* specimens, supported by the MACARBI project (IUEM). The authors are also grateful to the captain and crew of the RV Nereis II from the UMS Service at Sea of the OOB, for their help in acquiring N. cochlear shells. Analytical facilities (a part of the PANOPLY analytical Platform) at LSCE received funding from various sources (Région Ile-de-France; Commissariat à l’Energie Atomique; Institut National des Sciences de l’Univers/Centre National de la Recherche Scientifique; Université de Versailles/St-Quentin-en-Yvelines). Thoughtful comments by Editor W. Guo, S. Petersen, N. Meckler and one anonymous reviewer helped to improve the original version of the manuscript.

APPENDIX A. SUPPLEMENTARY MATERIAL

$\delta^{18}O_w$ measurements performed at the sampling site of the bivalves *Neopycnodonte cochlear* in the canyon Lacaze Duthiers at -270 m. Supplementary data to this article can be found online at https://doi.org/10.1016/j.gca.2021.09.019.

REFERENCES

Adkins J. F., Boyle E. A., Curry W. B. and Lutringer A. (2003) Stable isotopes in deep-sea corals and a new mechanisms for “vital effects”. *Geochim. Cosmochim. Acta* **67**, 1129–1143.

Affek H. P., Bar-Matthews M., Ayalon A., Matthews A. and Eiler J. M. (2008) Glacial/interglacial temperature variations in Soreq cave speleothems as recorded by ‘clumped isotope’thermometry. *Geochim. Cosmochim. Acta* **72**(22), 5351–5360.

Affek H. P. and Zaarur S. (2014) Kinetic isotope effect in CO_2 degassing: Insight from clumped and oxygen isotopes in laboratory precipitation experiments. *Geochim. Cosmochim. Acta* **143**, 319–330.

Anderson N. T., Kelson J. R., Kele S., Daëron M., Bonifacie M., Horita J., Mackey T. J., John C. M., Kluge T., Petsching P., Jost A. B., Huntington K. W., Bernasconi S. M. and Bergmann K. D. (2021) A unified clumped isotope thermometer calibration (0.5–1,100° C) using carbonate-based standardization. *Geophys. Res. Lett.* **48**(7), e2020GL092069.

Arkhipkin A., Boucher E., Gras M. and Brickle P. (2017) Variability in age and growth of common rock oyster *Saccostrea cucullata* (Bivalvia) in Ascension Island (central-east Atlantic). *J. Mar. Biol. Assoc. UK* **97**(4), 735–742.

Bajnai D., Fiebig J., Tomašových A., Garcia S. M., Rollion-Bard C., Raddatz J., Löffler N., Primo-Ramos C. and Brand U. (2018) Assessing kinetic fractionation in brachiopod calcite using clumped isotopes. *Sci. Rep.* **8**(1), 533.

Bernasconi S. M., Müller I. A., Bergmann K. D., Breitenbach S. F., Fernandez A., Hodell D. A., Jaggi M., Meckler A. N., Millan I. and Ziegler M. (2018) Reducing uncertainties in carbonate clumped isotope analysis through consistent carbonate-based standardization. *Geochem. Geophy. Geosy.* **19**(9), 2895–2914.

Bernasconi S. M., Daëron M., Bergmann K. D., Bonifacie M., Meckler A. N., Affek H. P., ... and Ziegler M. (2021) InterCarb: A community effort to improve interlaboratory standardization of the carbonate clumped isotope thermometer using carbonate standards. *Geochem. Geophys.* **22**(5) e2020GC009588.

Bonifacie M., Calmels D., Eiler J. M., Horita J., Chaduteau C., Vasconcelos C., Agrinier P., Katz A., Passey B. H., Ferry J. M. and Bourrand J. J. (2017) Calibration of the dolomite clumped isotope thermometer from 25 to 350° C, and implications for a universal calibration for all (Ca, Mg, Fe) CO_3 carbonates. *Geochim. Cosmochim. Ac.* **200**, 255–279.

Brand W. A., Assonov S. S. and Coplen T. B. (2010) Correction for the ^{17}O interference in $\delta(^{13}C)$ measurements when analyzing CO_2 with stable isotope mass spectrometry (IUPAC Technical Report). *Pure Appl. Chem.* **82**(8), 1719–1733.

Briard J., Pucéat E., Vennin E., Daëron M., Chavagnac V., Jaillet R., Merle D. and de Rafélis M. (2020) Seawater paleotemperature and paleosalinity evolution in neritic environments of the

Mediterranean margin: Insights from isotope analysis of bivalve shells. *Palaeogeogr. Palaeocl.* **543**, 109582.

Caldarescu D. E., Sadatzki H., Andersson C., Schäfer P., Fortunato H. and Meckler A. N. (2021) Clumped isotope thermometry in bivalve shells: A tool for reconstructing seasonal upwelling. *Geochim. Cosmochim. Acta* **294**, 174–191.

Came R. E., Brand U. and Affek H. P. (2014) Clumped isotope signatures in modern brachiopod carbonate. *Chem. Geol.* **377**, 20–30.

Carter J. G. (1980) Guide to bivalve shell microstructures. In *Skeletal growth of aquatic organisms* (eds. D. C. Rhoads and R. A. Lutz). Plenum Press, New York, pp. 645–673.

Chapron L., Le Bris N., Durrieu de Madron X., Peru E., Galand P. E. and Lartaud F. (2020) Long term monitoring of cold-water coral growth shows response to episodic meteorological events in the NW Mediterranean. *Deep-Sea Res. Pt. I* **160** 103255.

Chauvaud L., Lorrain A., Dunbar R. B., Paulet Y. M., Thouzeau G., Jean F., Guarini J.-M. and Mucciarone D. (2005) Shell of the Great Scallop *Pecten maximus* as a high-frequency archive of paleoenvironmental changes. *Geochem. Geophy. Geosy.* **6**(8), Q08001.

Cramer B. S., Miller K. G., Barrett P. J. and Wright J. D. (2011) Late Cretaceous-Neogene trends in deep ocean temperature and continental ice volume: Reconciling records of benthic foraminiferal geochemistry (δ^{18}O and Mg/Ca) with sea level history. *J. Geophys. Res.-Oceans* **116**(C12023).

Daëron M. (2021) Full propagation of analytical uncertainties in Δ_{47} measurements. *Geochem. Geophys.* **22**(5) e2020GC009592.

Daëron M., Guo W., Eiler J., Genty D., Blamart D., Boch R., Drysdale R., Maire R., Wainer K. and Zanchetta G. (2011) ^{13}C^{18}O clumping in speleothems: observations from natural caves and precipitation experiments. *Geochim. Cosmochim. Ac.* **75**(12), 3303–3317.

Daëron M., Blamart D., Peral M. and Affek H. P. (2016) Absolute isotopic abundance ratios and the accuracy of Δ_{47} measurements. *Chem. Geol.* **442**, 83–96.

Daëron M., Drysdale R. N., Peral M., Huyghe D., Blamart D., Coplen T. B., Lartaud F. and Zanchetta G. (2019) Most Earth-surface calcites precipitate out of equilibrium. *Nat. Commun.* **10** (1), 429.

Devriendt L. S., Watkins J. M. and McGregor H. V. (2017) Oxygen isotope fractionation in the $CaCO_3$-DIC-H_2O system. *Geochim. Cosmochim. Acta* **214**, 115–142.

de Winter N. J., Vellekoop J., Vorsselmans R., Golreihan A., Soete J., Petersen S. V., Meyer K. W., Casadio S., Speijer R. P. and Claeys P. (2018) An assessment of latest Cretaceous *Pycnodonte vesicularis* (Lamarck, 1806) shells as records for palaeoseasonality: a multi-proxy investigation. *Clim. Past.* **14**, 725–749.

de Winter N. J., Müller I. A., Kocken I. J., Thibault N., Ullmann C. V., Farnsworth A., Lunt D. L., Claeys P. and Ziegler M. (2021) Absolute seasonal temperature estimates from clumped isotopes in bivalve shells suggest warm and variable greenhouse climate. *Commun. Earth & Environ.* **2**(1), 1–8.

Defliese W. F., Hren M. T. and Lohmann K. C. (2015) Compositional and temperature effects of phosphoric acid fractionation on Δ_{47} analysis and implications for discrepant calibrations. *Chem. Geol.* **396**, 51–60.

Dennis K. J., Affek H. P., Passey B. H., Schrag D. P. and Eiler J. M. (2011) Defining an absolute reference frame for 'clumped'isotope studies of CO_2. *Geochim. Cosmochim. Ac.* **75** (22), 7117–7131.

Durrieu de Madron X., Houpert L., Puig P., Sanchez-Vidal A., Testor P., Bosse A., Estournel C., Somot S., Bourrin F., Bouin M. N., Beauverger M., Beguery L., Calafat A., Canals M., Cassou C., Coppola L., Dausse D., D'Ortenzio F., Font J., Heussner L., Kunesch S., Lefevre D., Le Goff H., Martin J., Mortier L., Palanques A. and Raimbault P. (2013) Interaction of dense shelf water cascading and open-sea convection in the northwestern Mediterranean during winter 2012. *Geophys. Res. Lett.* **40**(7), 1379–1385.

Eagle R. A., Eiler J. M., Tripati A. K., Ries J. B., Freitas P. S., Hiebenthal C., Wanamaker, Jr., A. D., Taviano M., Elliot M., Marenssi S., Nakamura K., Ramirez P. and Roy K. (2013) The influence of temperature and seawater carbonate saturation state on ^{13}C–^{18}O bond ordering in bivalve mollusks. *Biogeosciences* **10**, 4591–4606.

Eiler J. M. (2011) Paleoclimate reconstruction using carbonate clumped isotope thermometry. *Quaternary Sci. Rev.* **30**(25–26), 3575–3588.

Epstein S. and Mayeda T. (1953) Variation of ^{18}O content of waters from natural sources. *Geochim. Cosmochim. Ac.* **4**, 213–224.

Fenger T., Surge D., Schöne B. and Milner N. (2007) Sclerochronology and geochemical variation in limpet shells (Patella vulgata), a new archive to reconstruct Holocene coastal sea surface temperature. *Geochem. Geophy. Geosy.* **8**, Q07001.

Fernandez A., Müller I. A., Rodríguez-Sanz L., van Dijk J., Looser N. and Bernasconi S. M. (2017) A reassessment of the precision of carbonate clumped isotope measurements: Implications for calibrations and paleoclimate reconstructions. *Geochem. Geophys.* **18**(12), 4375–4386.

Gentry D. K., Sosdian S., Grossman E. L., Rosenthal Y., Hicks D. and Lear C. H. (2008) Stable isotope and Sr/Ca profiles from the marine gastropod *Conus ermineus*: testing a multiproxy approach for inferring paleotemperature and paleosalinity. *Palaios* **23**(4), 195–209.

Ghosh P., Adkins J., Affek H., Balta B., Guo W., Schauble E. A., Schrag D. and Eiler J. M. (2006) ^{13}C–^{18}O bonds in carbonate minerals: a new kind of paleothermometer. *Geochim. Cosmochim. Acta* **70**(6), 1439–1456.

Ghosh P., Prasanna K., Banerjee Y., Williams I. S., Gagan M. K., Chaudhuri A. and Suwas S. (2018) Rainfall seasonality on the Indian subcontinent during the Cretaceous greenhouse. *Sci. Rep.* **8**(1), 1–9.

Gillikin D. P., Lorrain A., Meng L. and Dehairs F. (2007) A large metabolic carbon contribution to the δ^{13}C record in marine aragonitic bivalve shells. *Geochim. Cosmochim. Acta* **71**(12), 2936–2946.

Grauel A. L., Schmid T. W., Hu B., Bergami C., Capotondi L., Zhou L. and Bernasconi S. M. (2013) Calibration and application of the 'clumped isotope' thermometer to foraminifera for high-resolution climate reconstructions. *Geochim. Cosmochim. Ac.* **108**, 125–140.

Guo W. (2020) Kinetic clumped isotope fractionation in the DIC-H_2O-CO_2 system: Patterns, controls, and implications. *Geochim. Cosmochim. Ac.* **268**, 230–257.

Harzhauser M., Piller W. E., Müllegger S., Grunert P. and Micheels A. (2010) Changing seasonality patterns in Central Europe from Miocene Climate Optimum to Miocene Climate Transition deduced from the *Crassostrea* isotope archive. *Global Planet. Change* **76**, 77–84.

Henkes G. A., Passey B. H., Wanamaker, Jr, A. D., Grossman E. L., Ambrose, Jr, W. G. and Carroll M. L. (2013) Carbonate clumped isotope compositions of modern marine mollusk and brachiopod shells. *Geochim. Cosmochim. Ac.* **106**, 307–325.

Hill P. S., Tripati A. K. and Schauble E. A. (2014) Theoretical constraints on the effects of pH, salinity, and temperature on clumped isotope signatures of dissolved inorganic carbon species and precipitating carbonate minerals. *Geochim. Cosmochim. Acta* **125**, 610–652.

Huyghe D., de Rafelis M., Ropert M., Mouchi V., Emmanuel L., Renard M. and Lartaud F. (2019) New insights into oyster high-resolution hinge growth patterns. *Mar. Biol.* **166**, 48.

Huyghe D., Emmanuel L., de Rafelis M., Ropert M., Renard M., Labourdette N. and Lartaud F. (2020) Oxygen isotope disequilibrium in the juvenile portion of oyster shells biases seawater temperature reconstructions. *Estuar. Coast. Shelf S.* **240** 106777.

Hren M. T., Sheldon N. D., Grimes S. T., Collinson M. E., Hooker J. J., Bugler M. and Lohmann K. C. (2013) Terrestrial cooling in Northern Europe during the Eocene-Oligocene transition. *P. Natl. Acad. Sci. U.S.A.* **110**(19), 7562–7567.

Katz A., Bonifacie M., Hermoso M., Cartigny P. and Calmels D. (2017) Laboratory-grown coccoliths exhibit no vital effect in clumped isotope (Δ_{47}) composition on a range of geologically relevant temperatures. *Geochim. Cosmochim. Ac.* **208**, 335–353.

Kele S., Breitenbach S. F., Capezzuoli E., Meckler A. N., Ziegler M., Millan I. M., Kluge T., Deak J., Hanselmann K., John C. M., Yan H., Liu Z. and Bernasconi S. (2015) Temperature dependence of oxygen-and clumped isotope fractionation in carbonates: A study of travertines and tufas in the 6–95 C temperature range. *Geochim. Cosmochim. Ac.* **168**, 172–192.

Kelson J. R., Huntington K. W., Schauer A. J., Saenger C. and Lechler A. R. (2017) Toward a universal carbonate clumped isotope calibration: Diverse synthesis and preparatory methods suggest a single temperature relationship. *Geochim. Cosmochim. Ac.* **197**, 104–131.

Killingley J. S. and Newman W. A. (1982) ^{18}O fractionation in barnacle calcite, a barnacle paleotemperature equation. *J. Mar. Res.* **40**, 893–901.

Kim S. T., Mucci A. and Taylor B. E. (2007) Phosphoric acid fractionation factors for calcite and aragonite between 25 and 75 C: revisited. *Chem. Geol.* **246**(3–4), 135–146.

Kim S. T. and O'Neil J. R. (1997) Equilibrium and nonequilibrium oxygen isotope effects in synthetic carbonates. *Geochim. Cosmochim. Ac.* **61**(16), 3461–3475.

Kirby M. X., Soniat T. M. and Spero H. J. (1998) Stable isotope sclerochronology of Pleistocene and recent oyster shells (*Crassostrea virginica*). *Palaios* **13**, 560–569.

Kobashi T., Grossman E. L., Yancey T. E. and Dockery D. T. (2001) Reevaluation of conflicting Eocene tropical temperature estimates: Molluskan oxygen evidence for warm low latitudes. *Geology* **29**, 983–986.

Langlet D., Alunno-Bruscia M., Rafélis M., Renard M., Roux M., Schein E. and Buestel D. (2006) Experimental and natural cathodoluminescence in the shell of *Crassostrea gigas* from Thau lagoon (France): ecological and environmental implications. *Mar. Ecol. Progr. Ser.* **317**, 143–156.

Lartaud F., Langlet D., de Rafelis M., Emmanuel L. and Renard M. (2006) Description of seasonal rythmicity in fossil oyster shells *Cassostrea aginensis* Tournouer, 1914 (Aquitanian) and *Ostrea bellovacina* Lamarck, 1806 (Thanetian). Cathodoluminescence and sclerochronological approaches. *Geobios* **39**(6), 845–852.

Lartaud F., Chauvaud L., Richard J., Toulot A., Bollinger C., Testu L. and Paulet Y. M. (2010a) Experimental growth pattern calibration of Antarctic scallop shells (Adamussium colbecki, Smith 1902) to provide a biogenic archive of high-resolution records of environmental and climatic changes. *J Exp. Mar. Biol. Ecol.* **393**(1–2), 158–167.

Lartaud F., de Rafélis M., Ropert M., Emmanuel L., Geairon P. and Renard M. (2010b) Mn labelling of living oysters: artificial and natural cathodoluminescence analyses as a tool for age and growth rate determination of *C. gigas* (Thunberg, 1793) shells. *Aquaculture* **300**(1), 206–217.

Lartaud F., Emmanuel L., de Rafelis M., Ropert M., Labourdette N., Richardson C. A. and Renard M. (2010c) A latitudinal gradient of seasonal temperature variation recorded in oyster shells from the coastal waters of France and The Netherlands. *Facies* **56**, 13–25.

Lartaud F., Emmanuel L., de Rafélis M., Pouvreau S. and Renard M. (2010d) Influence of food supply on the δ^{13}C signature of mollusc shells: implications for palaeoenvironmental reconstitutions. *Geo-Mar. Lett.* **30**(1), 23–34.

LeGrande A. N. and Schmidt G. A. (2006) Global gridded data set of the oxygen isotopic composition in seawater. *Geophys. Res. Lett.* **33**(12).

Marin F. and Luquet G. (2004) Molluscan shell proteins. *C. R. Palevol.* **3**(6–7), 469–492.

McClanahan T. R., Ateweberhan M., Muhando C. A., Maina J. and Mohammed M. S. (2007) Effects of climate and seawater temperature variation on coral bleaching and mortality. *Ecol. Monogr.* **77**(4), 503–525.

McConnaughey T. (1989) ^{13}C and ^{18}O isotopic disequilibrium in biological carbonates: I. Patterns. *Geochim. Cosmochim. Ac.* **53** (1), 151–162.

McConnaughey T. A., Burdett J., Whelan J. F. and Paull C. K. (1997) Carbon isotopes in biological carbonates: respiration and photosynthesis. *Geochim. Cosmochim. Acta* **61**(3), 611–622.

Meinicke N., Ho S. L., Hannisdal B., Nürnberg D., Tripati A., Schiebel R. and Meckler A. N. (2020) A robust calibration of the clumped isotopes to temperature relationship for foraminifers. *Geochim. Cosmochim. Ac.* **270**, 160–218.

Meckler A. N., Affolter S., Dublyansky Y. V., Krüger Y., Vogel N., Bernasconi S. M., Frenz M., Kipfer R., Leuenberger M., Spötl C., Carolin S., Cobb K. M., Moerman J., Adkins J. and Fleitmann D. (2015) Glacial–interglacial temperature change in the tropical West Pacific: A comparison of stalagmite-based paleo-thermometers. *Quat. Sci. Rev.* **127**, 90–116.

Mitchell L., Fallick A. E. and Curry G. B. (1994) Stable carbon and oxygen isotope compositions of mollusc shells from Britain and New Zealand. *Palaeogeogr. Palaeocl.* **111**, 207–216.

Mouchi V., de Rafélis M., Lartaud F., Fialin M. and Verrecchia E. (2013) Chemical labelling of oyster shells used for time-calibrated high-resolution Mg/Ca ratios: a tool for estimation of past seasonal temperature variations. *Palaeogeogr. Palaeocl.* **373**, 66–74.

Owen R., Kennedy H. and Richardson C. (2002) Isotopic partitioning between scallop shell calcite and seawater: effect of shell growth rate. *Geochim. Cosmochim. Ac.* **66**(10), 1727–1737.

Peral M., Daëron M., Blamart D., Bassinot F., Dewilde F., Smialkowski N., Isguder G., Bonnin J., Jorissen F., Kissel C., Michel E., Vazquez Riveiros N. and Waelbroeck C. (2018) Updated calibration of the clumped isotope thermometer in planktonic and benthic foraminifera. *Geochim. Cosmochim. Ac.* **239**, 1–16.

Petersen S. V., Defliese W. F., Saenger C., Daëron M., Huntington K. W., John C. M., Kelson J. R., Bernasconi S. M., Colman A. S., Kluge T., Olack G. A., Schauer A. J., Bajnai D., Bonifacie M., Breitenbach S. F. M., Fiebig J., Fernandez A. B., Henkes G. A., Hodell D., Katz A., Kele S., Lohmann K. C., Passey B. H., Peral M. Y., Petrizzo D. A., Rosenheim B. E., Tripati A., Venturelli R., Young E. D. and Winkelstern I. Z. (2019) Effects of improved ^{17}O correction on interlaboratory agreement in clumped isotope calibrations, estimates of mineral-specific offsets, and temperature dependence of acid digestion fractionation. *Geochem. Geophy. Geosy.* **20**(7), 3495–3519.

Petrizzo D. A., Young E. D. and Runnegar B. N. (2014) Implications of high-precision measurements of ^{13}C–^{18}O bond ordering in CO_2 for thermometry in modern bivalved mollusc shells. *Geochim. Cosmochim. Ac.* **142**, 400–410.

Piasecki A., Bernasconi S. M., Grauel A. L., Hannisdal B., Ho S. L., Leutert T. J., Marchitto T. M., Meinicke N., Tisserand A. and Meckler N. (2019) Application of clumped isotope thermometry to benthic foraminifera. *Geochem. Geophy. Geosy.* **20**(4), 2082–2090.

Prahl F. G. and Wakeham S. G. (1987) Calibration of unsaturation patterns in long-chain ketone compositions for palaeotemperature assessment. *Nature* **330**(6146), 367–369.

Purton L. and Brasier M. (1997) Gastropod carbonate $\delta^{18}O$ and $\delta^{13}C$ values record strong seasonal productivity and stratification shifts during the late Eocene in England. *Geology* **25**(10), 871–874.

Rollion-Bard C. and Blamart D. (2015) Possible controls on Li, Na, and Mg incorporation into aragonite coral skeletons. *Chem. Geol.* **396**, 98–111.

Salvi D. and Mariottini P. (2017) Molecular taxonomy in 2D: a novel ITS2 rRNA sequence-structure approach guides the description of the oysters' subfamily Saccostreinae and the genus *Magallana* (Bivalvia: Ostreidae). *Zool. J. Linn. Soc.-Lond.* **179**, 263–276.

Schauble E. A., Ghosh P. and Eiler J. M. (2006) Preferential formation of ^{13}C–$^{1}8O$ bonds in carbonate minerals, estimated using first-principles lattice dynamics. *Geochim. Cosmochim. Ac.* **70**(10), 2510–2529.

Schauer A. J., Kelson J., Saenger C. and Huntington K. W. (2016) Choice of ^{17}O correction affects clumped isotope (Δ_{47}) values of CO_2 measured with mass spectrometry. *Rapid Commun. Mass Sp.* **30**(24), 2607–2616.

Schouten S., Forster A., Panoto F. E. and Damsté J. S. S. (2007) Towards calibration of the TEX_{86} palaeothermometer for tropical sea surface temperatures in ancient greenhouse worlds. *Org. Geochem.* **38**(9), 1537–1546.

Shackleton N. (1967) Oxygen isotope analyses and Pleistocene temperatures reassessed. *Nature* **215**(5096), 15.

Spooner P. T., Guo W., Robinson L. F., Thiagarajan N., Hendry K. R., Rosenheim B. E. and Leng M. J. (2016) Clumped isotope composition of cold-water corals: A role for vital effects? *Geochim. Cosmochim. Ac.* **179**, 123–141.

Srivastava R., Ramesh R., Prakash S., Anilkumar N. and Sudhakar M. (2007) Oxygen isotope and salinity variations in the Indian sector of the Southern Ocean. *Geophys. Res. Lett.* **34**, L24603.

Surge D., Lohmann K. C. and Dettman D. L. (2001) Controls on isotopic chemistry of the American oyster, Crassostrea virginica: implications for growth patterns. *Palaeogeogr. Palaeocl.* **172**, 283–296.

Thomsen J., Haynert K., Wegner K. M. and Melzner F. (2015) Impact of seawater carbonate chemistry on the calcification of marine bivalves. *Biogeosciences* **12**(14), 4209–4220.

Thiagarajan N., Adkins J. and Eiler J. (2011) Carbonate clumped isotope thermometry of deep-sea corals and implications for vital effects. *Geochim. Cosmochim. Ac.* **75**(16), 4416–4425.

Tripati A. K., Eagle R. A., Thiagarajan N., Gagnon A. C., Bauch H., Halloran P. R. and Eiler J. M. (2010) ^{13}C–^{18}O isotope signatures and 'clumped isotope' thermometry in foraminifera and coccoliths. *Geochim. Cosmochim. Ac.* **74**(20), 5697–5717.

Tynan S., Dutton A., Eggins S. and Opdyke B. (2014) Oxygen isotope records of the Australian flat oyster (Ostrea angasi) as a potential temperature archive. *Mar. Geol.* **357**, 195–209.

Tynan S., Opdyke B. N., Walczak M., Eggins S. and Dutton A. (2017) Assessment of Mg/Ca in Saccostrea glomerata (the Sydney rock oyster) shell as a potential temperature record. *Palaeogeogr. Palaeoclimatol. Palaeoecol.* **484**, 79–88.

Ullmann C. V., Wiechert U. and Korte C. (2010) Oxygen isotope fluctuations in a modern North Sea oyster (*Crassostrea gigas*) compared with annual variations in seawater temperature: Implications for palaeoclimate studies. *Chem. Geol.* **277**(1), 160–166.

Uvanović H., Schöne B. R., Markulin K., Janeković I. and Peharda M. (2021) Venerid bivalve Venus verrucosa as a high-resolution archive of seawater temperature in the Mediterranean Sea. *Palaeogeogr. Palaeocl.* **561** 110057.

Van Plantinga A. A. and Grossman E. L. (2018) Stable and clumped isotope sclerochronologies of mussels from the Brazos River, Texas (USA): Environmental and ecologic proxy. *Chem. Geol.* **502**, 55–65.

Watkins J. M. and Hunt J. D. (2015) A process-based model for non-equilibrium clumped isotope effects in carbonates. *Earth Planet. Sci. Lett.* **432**, 152–165.

Wefer G. and Berger W. H. (1991) Isotope paleontology: growth and composition of extant calcareous species. *Mar. Geol.* **100**, 207–248.

Wisshak M., Correa M. L., Gofas S., Salas C., Taviani M., Jakobsen J. and Freiwald A. (2009) Shell architecture, element composition, and stable isotope signature of the giant deep-sea oyster *Neopycnodonte zibrowii* sp. n. from the NE Atlantic. *Deep-Sea Res. Pt. I* **56**(3), 374–407.

York D., Evensen N. M., López Martínez M. and De Basabe Delgado J. (2004) Unified equations for the slope, intercept, and standard errors of the best straight line. *Am. J. Phys.* **72**(3), 367–375.

Zaarur S., Olack G. and Affek H. P. (2011) Paleo-environmental implication of clumped isotopes in land snail shells. *Geochim. Cosmochim. Ac.* **75**(22), 6859–6869.

Zhai J., Wang X., Qin B., Cui L., Zhang S. and Ding Z. (2019) Clumped isotopes in land snail shells over China: Towards establishing a biogenic carbonate paleothermometer. *Geochim. Cosmochim. Ac.* **257**, 68–79.

Zhang N., Yamada K., Kano A., Matsumoto R. and Yoshida N. (2018) Equilibrated clumped isotope signatures of land-snail shells observed from laboratory culturing experiments and its environmental implications. *Chem. Geol.* **488**, 189–199.

Associate editor: Weifu Guo